BMC Cardiovascular Disorders

RESEARCH

Open Access

Long QT syndrome type 1: clinical and functional characterization of *KCNQ1* variant c.1111G > C

Neringa Bileisiene[1,2*], Anastasiia Shelest[3], Gunda Petraityte[4], Aidas Alaburda[3], Ausra Sasnauskiene[3], Andrius Jasinevicius[3], Visvaldas Kairys[5], Justas Dapkunas[5], Violeta Mikstiene[2,4], Vilmante Zitkute[3], Zivile Maldziene[2,4], Jurate Barysiene[1,2] and Egle Preiksaitiene[2,4]

Abstract

Background Congenital long QT syndrome is a clinical disorder of genetic origin characterized by delayed repolarization of the myocardium, electrocardiographic QT prolongation, and increased risk of syncope, and sudden cardiac death due to polymorphic ventricular tachycardia. *KCNQ1*-related congenital long QT syndrome (LQT1) is the most prevalent of the long QT syndrome genetic subgroups and is typically caused by pathogenic missense or protein-truncating gene variants. Phenotypic features, computational analysis, and electrophysiological characterization of the variant are essential steps in assessing the pathogenicity of DNA variants and contribute to the future management of patients.

Methods We report the results of the clinical evaluation of five Lithuanian families with a rare pathogenic heterozygous *KCNQ1* variant c.1111G > C [p.(Ala371Pro)], including computational Kv7.1 protein structure analysis, molecular dynamics simulations, and electrophysiological characterization of the affected Kv7.1 channel.

Results The individuals with the pathogenic variant ($n = 9$) exhibited phenotypic LQTS features during an exercise stress test (mean QTc during peak exercise was 497 ± 26 ms; mean QTc during the 4th minute of the recovery – 485 ± 22 ms) despite the low penetrance in the resting 12-lead ECG (mean QTc 423 ± 37 ms) or their symptomatic status. The sudden cardiac deaths of two females at the age of 34 years were reported in these families. Molecular dynamics simulations showed that the change p.Ala371Pro might disrupt the structure of the helix A in the Kv7.1 protein. Functional evaluation revealed that the pathogenic variant reduced the conductance of the channel by 46%, while the voltage dependence of activation was not affected.

Conclusions This is the first functional description of the *KCNQ1* variant c.1111G > C that causes LQT1 phenotypic features. The variant is highly suggestive of the risk of disease-related cardiac events, particularly under adrenergic urge.

Keywords Long QT syndrome type 1, KCNQ1, C-terminus pathogenic variant, KCNQ1/KCNE1 channel, $K_v7.1$, I_{Ks}

*Correspondence:
Neringa Bileisiene
neringa.bileisiene@mf.vu.lt
[1]Clinic of Cardiac and Vascular Diseases, Institute of Clinical Medicine, Faculty of Medicine, Vilnius University, Vilnius, Lithuania
[2]Vilnius University Hospital Santaros Klinikos, Vilnius, Lithuania
[3]Institute of Biosciences, Life Sciences Center, Vilnius University, Vilnius, Lithuania
[4]Department of Human and Medical Genetics, Institute of Biomedical Sciences, Faculty of Medicine, Vilnius University, Vilnius, Lithuania
[5]Institute of Biotechnology, Life Sciences Center, Vilnius University, Vilnius, Lithuania

© The Author(s) 2025. **Open Access** This article is licensed under a Creative Commons Attribution-NonCommercial-NoDerivatives 4.0 International License, which permits any non-commercial use, sharing, distribution and reproduction in any medium or format, as long as you give appropriate credit to the original author(s) and the source, provide a link to the Creative Commons licence, and indicate if you modified the licensed material. You do not have permission under this licence to share adapted material derived from this article or parts of it. The images or other third party material in this article are included in the article's Creative Commons licence, unless indicated otherwise in a credit line to the material. If material is not included in the article's Creative Commons licence and your intended use is not permitted by statutory regulation or exceeds the permitted use, you will need to obtain permission directly from the copyright holder. To view a copy of this licence, visit http://creativecommons.org/licenses/by-nc-nd/4.0/.

Background

Congenital long QT syndrome (LQTS) (ORPHA:101016) is the first described and most common cardiac channelopathy. It is a clinical disorder of genetic origin characterized by delayed repolarization of the myocardium, electrocardiographic QT prolongation, and heightened risk of syncope, and sudden cardiac death due to polymorphic ventricular tachycardia known as Torsades de Pointes [1]. Pathogenic variants in the *KCNQ1* (MIM#607542), *KCNH2* (MIM#152427), and *SCN5A* (MIM#600163) genes are the leading causes of the disease. *KCNQ1*-related LQTS (MIM#192500) comprises 45% of the disease and is the most prevalent of the three major LQTS genetic subgroups [2].

KCNQ1 encodes the voltage-gated potassium channel α-subunit (Kv7.1, UniProtKB P51787), which is responsible for the slow-activating, late-repolarizing potassium current (I_{Ks}) in the human heart. Kv7.1 forms homotetramers and assembles with the β-subunit encoded by *KCNE1* [3]. Each Kv7.1 monomer contains an intracellular N-terminal helix (residues 1–121), six membrane-spanning segments with a voltage-sensing domain and a pore domain (residues 122–348), and four intracellular C-terminal helices A–D (residues 349–676) [4]. The function of the channel is regulated by KCNE1, calmodulin, and other regulators [5, 6].

Pathogenic variants in *KCNQ1* can cause *KCNQ1*-related LQTS and other phenotypes. Protein-truncating and missense variants are known to be causative. However, genotype–phenotype correlations are unclear, and there is still a lack of knowledge of how pathogenic variants change channel structure and function. Electrophysiological characterization of ion channel alterations is increasingly recognized as a critical step in assessing the pathogenicity of DNA variants, particularly missense variants. Functional testing provides essential biophysical evidence to support genotype–phenotype relationships and to ensure that genetic findings are clinically relevant [7].

We report on the *KCNQ1* variant NM_000218.3:c.1111G > C, NP_000209.2:p.(Ala371Pro), (rs199473412), which was identified in five seemingly unrelated Lithuanian families tested due to LQTS. Clinical features of variably affected adults, the results of protein modelling and electrophysiological experiments are presented.

Materials and methods

Enrolment and clinical evaluation

Five Lithuanian families (Fig. 1, Suppl. Mat. 1) with the rare pathogenic *KCNQ1* variant NM_000218.3:c.1111G > C were identified at Vilnius University Hospital Santaros Klinikos. A comprehensive clinical evaluation of nine adults was performed between December 2022 and December 2023 during their follow-up according to the study protocol. The study was approved by the Regional Committee for Biomedical Research Ethics. All subjects gave their written informed consent. The investigation was conducted according to the principles of the Helsinki Declaration. Clinical evaluation included anamnesis of disease-related symptoms, collection of family history, 12-lead ECGs at rest in a supine position and at brisk standing, transthoracic echocardiography with left ventricle (LV) strain analysis, and exercise stress test (EST) (Suppl. Mat. 2).

Next-generation sequencing

Next-generation sequencing analysis of the probands` peripheral blood genomic DNA (III-1 from the 2nd family and II-1 from the 5th family, Fig. 1) was performed using the TruSight Cardio Sequencing panel (Illumina Inc., San Diego, CA). One hundred seventy genes were analyzed, including the genes associated with prolonged QT (Suppl. Mat. 3). Prepared DNA libraries were sequenced on the Illumina MiSeq system. Data analysis

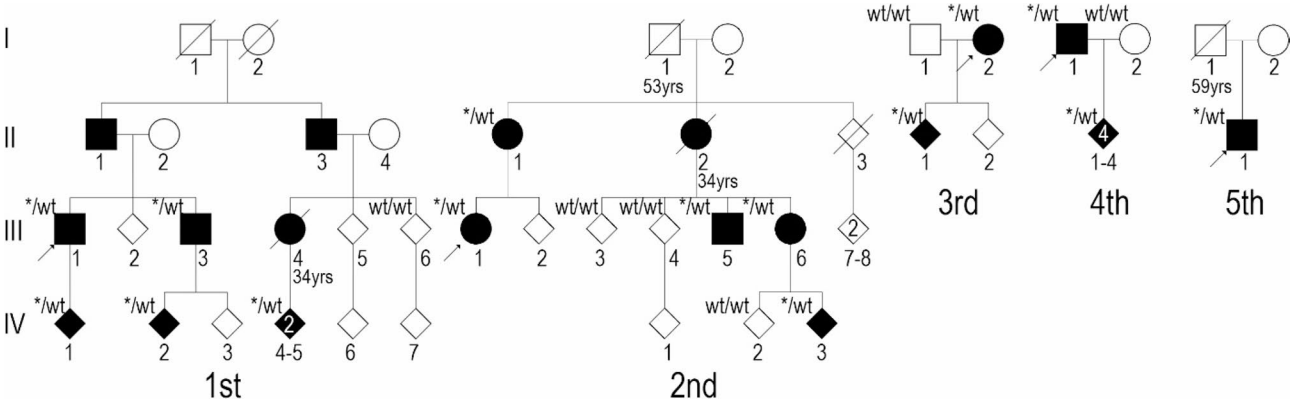

Fig. 1 Genealogies of 1st-5th families. Arrows indicate probands. Black symbols show affected individuals. Asterisks indicate a *KCNQ1* variant NM_000218.3:c.1111G > C, NP_000209.2:p.Ala371Pro (rs199473412). WT – wild type. A diamond shape indicates unspecified gender

was performed using a standard Illumina bioinformatic workflow. The variants were analyzed and annotated using VariantStudio 3.0 software. In silico analysis of the variants was performed using Mutation Taster [8], PolyPhen-2 [9], SIFT Human Protein [10], and similar tools.

Polymerase chain reactions and Sanger sequencing

Polymerase chain reaction (PCR) was performed on gDNA regions flanking the *KCNQ1* variant NM_000218.3:c.1111G > C, NP_000209.2:p.(Ala371Pro), (rs199473412) in the remaining adult samples, using primers designed with the Primer-Blast tool [11]. The resulting PCR products were sequenced using the BigDye® Terminator v3.1 Cycle Sequencing Kit (Thermo Fisher Scientific, USA) and ABI 3130xL Genetic Analyser (Thermo Fisher Scientific, USA). The obtained sequences were then aligned with the reference sequence of the *KCNQ1* (NCBI: NM_ 000218.3).

Analysis of protein structure and molecular dynamics simulations

Protein sequence was downloaded from the UniProt database (UniProt: P51787) [12]. Structural data on protein interactions were queried and analyzed using the PPI3D web server [13]. The structure models for the fragment of KCNQ1-calmodulin interaction (involving only helices HA and HB from KCNQ1) containing Ala371Pro and Ala371Thr variants were generated by homology modelling in the PPI3D web server [14] using PDB structure 6V00 as a template [15].

Molecular dynamics simulations were performed using GROMACS software (2020.4 version) [16], using CHARMM36m parameters for the protein (July 2021 version) [17]. The protein was placed in a dodecahedral periodic simulation box with a 10 Å distance between the protein and the box boundary. The box was filled with CHARMM-modified TIP3P water molecules [18] and several sodium and chloride ions to recreate a 0.15 M salt concentration and to keep the system neutral. To explore the reproducibility of the results, three different copies of the same system were created with a different initial placement of ions using different random seeds. The clashes in the assembled protein-solvent system were removed by performing steepest descent optimization until the maximum force threshold on any of the atoms reached 1000 $kJ \times mol^{-1} \times nm^{-1}$. Afterwards, the system underwent 100 picosecond NVT (constant number of particles, constant volume, constant temperature) equilibration using 2 fs time steps at 300 K temperature, with the positions of the nonhydrogen atoms of the protein constrained in space, allowing the protein hydrogens, water solvent and ions to relax and rearrange. The final step, a 500 ns constant temperature production run for each of the three copies, was carried out using the following settings/parameters: 2 fs time steps; V-rescaling algorithm for the temperature coupling with $\tau_T = 0.1$ ps time constant, using the protein atoms versus the rest of the system as two coupled groups; Parrinello-Rahman algorithm for the pressure coupling with $\tau_p = 2$ ps time constant and 4.5×10^{-5} bar^{-1} isothermal compressibility for water; Verlet cutoff scheme; Particle Mesh Ewald (PME) algorithm for the electrostatic interactions with a 1.2 nm cutoff and 4th-order cubic interpolation with 0.16 nm grid spacing for Fast Fourier Transform; 1.2 nm cutoff for the van der Waals interactions; snapshots recorded to the hard drive with 1 ns interval. The resulting trajectories were analyzed using the Bio3D library (version 2.4.5) in R [19]. The structural elements of the trajectories were analyzed using DSSP program (v. 4.5.6) [20]. The amino residue contacts were analyzed using Voronota-JS expansion of Voronota software (v. 1.29.4307) [21].

Plasmid mutagenesis and bacterial cloning

For wild type KCNQ1 expression, plasmid pIRES(A7Mut) CyOFP1_KCNQ1 was used, it was a gift from Al George (Addgene plasmid # 173162; http://n2t.net/addgene:173162; RRID: Addgene_173162). *KCNQ1* variant NM_000218.3: c.1111G > C was created following the Thermo Scientific site-directed mutagenesis protocol, according to the manufacturer's guidelines. Bacterial colonies were screened by PCR and restriction analysis. Altered sequence region was verified by Sanger sequencing.

Cell transfection

Human embryonic kidney (HEK293T/17) cells (ATCC) were seeded in 24-well plates (Thermo Scientific Biolite 24-well Multidish) at 80,000 cells/ml density, a day before the transfection. According to the manufacturer's protocol, the Lipofectamine® 3000 Transfection Reagent (Thermo Fisher Scientific) was used for transient transfection. KCNE1 coding plasmid was pIRES_EGFP_GA_KCNE1, it was a gift from Al George (Addgene plasmid # 173160; http://n2t.net/addgene:173160; RRID: Addgene_173160). Cells were transfected with different plasmid combinations (KCNQ1_wt; KCNQ1_mut; KCNQ1_wt + KCNE1, KCNQ1_mut + KCNE1), maintaining the plasmid DNA amount recommended by manufacturer. After transfection, cells were incubated (37 °C, 5% CO_2) and allowed to express the transgene for 24–48 h before electrophysiological analysis.

Electrophysiological recording

Whole-cell voltage-clamp recordings were performed on human embryonic kidney (HEK293) cells transfected with wild-type KCNQ1 (WT) or with the KCNQ1 p.(Ala371Pro) variant (A371P), together with the KCNE1 subunit. The HEK293 cell line was chosen due

to its consistent morphology [22], adhesion characteristics [23], and widespread use in ion channel research [24], making it a well-established model for functional analysis. Plasmids co-expressing KCNQ1 (together with CyOFP1) and KCNE1 (together with EGFP) were used to identify transfected cells for the voltage-clamp recordings. Cells exhibiting fluorescence, indicating successful transfection, were selected for the electrophysiological recordings.

Recordings were conducted at room temperature (21 ± 1 °C) 2–3 days post-transfection using a Multiclamp 700B amplifier (Molecular Devices) controlled by pCLAMP 10.5 software (Molecular Devices). Patch microelectrodes were pulled from borosilicate glass capillaries using a Flaming/Brown micropipette puller (Model P-1000; Sutter Instrument Co., USA) and had a resistance of 2–4 MΩ when filled with the intracellular solution.

The intracellular solution contained (in mM): 140 KCl, 1 Na2-ATP, 2 EGTA, 10 HEPES, 0.1 CaCl2, 1 MgCl2, and 10 glucose, with pH adjusted to 7.4 using KOH. The extracellular solution contained (in mM): 140 NaCl, 4 KCl, 2 CaCl2, 1 MgCl2, 10 HEPES, and 10 glucose, with pH adjusted to 7.4 using NaOH. Chromanol 293B, dissolved in DMSO at a final concentration of 10 µM, was used as a specific inhibitor of KCNQ1 channels.

Membrane currents were recorded using the voltage-clamp protocol that starts from a holding potential of -90 mV and depolarizing steps of 2-s duration and applied in 20 mV increments up to + 70 mV. The steady current values at the end of a 2-s pulse were used for evaluation. The activation threshold for the KCNQ1 current was near – 40 mV [25]. To assess leak conductance, currents at three subthreshold potentials (-90, -70, and – 50 mV) were used for the linear extrapolation of leak currents at -30– +70 mV. Leak subtraction resulted in the isolation of the voltage-dependent current component. The voltage-dependent current components were normalized to the cell membrane capacitance to obtain current densities (pA/pF).

Current densities were also used to generate conductance-voltage (G-V) curves to determine the voltage dependence of channel activation. To obtain G-V curves, the change in current (ΔI) was divided by the change in membrane potential (ΔV) at each voltage step. The G_{max} and $V_{1/2}$ were obtained by fitting the G-V curve with a Boltzmann equation (Origin Pro).

$$G(V) = G_{min} + \frac{(G_{max} - G_{min})}{1 + \exp\left(\frac{V - V_{1/2}}{s}\right)} \quad (1)$$

G_{min} is the minimal conductance, G_{max} is the maximal conductance, $V_{1/2}$ is the voltage where 50% of the maximal conductance level is reached and s is the slope factor.

The Shapiro-Wilk test (Origin Pro) was used to assess normality. Since the data did not follow a normal distribution, statistical analysis was performed using the non-parametric Kruskal-Wallis test (Origin Pro) to evaluate statistically significant differences among multiple groups. The Mann-Whitney U test (Origin Pro) assessed statistically significant differences between the two groups. Statistical significance was defined as $p \le 0.05$. In the figures, significance levels are indicated as follows: $^{*}p \le 0.05$, $^{***}p \le 0.005$. Results are presented as mean ± standard error, with "n" representing the number of cells.

Results

Clinical evaluation

The demographic, clinical and electromechanical characteristics of individuals with the heterozygous *KCNQ1* variant c.1111G > C were analyzed (Table 1). Nine adults with an insignificant predominance of males (56%) were included in the study; the mean age of the patients was 33.4 ± 10.8 years. Four patients (44%) were considered symptomatic: one had multiple syncopal episodes during physical activity (playing competitive sports games), and the other three experienced arrhythmical presyncope, provoked by physical exertion. Manifestation of the disease-related symptoms was observed from childhood to puberty within the range of 10 to 16 years. Between the molecular diagnosis and clinical investigation (mean 3.7 ± 1.3 years), all patients were asymptomatic, though four patients (44%) were taking beta-blockers (propranolol). Sudden cardiac deaths were observed in three out of five unrelated LQT1 families: the deaths of females at the age of 34 years (II-2, 2nd family; III-4, 1st family, both obligatory had a familial variant), the death of the male at 53 years of age (I-1, 2nd family) and male at the age of 59 years (I-1, 5th family). During clinical evaluation, penetration in the 12-lead ECG at rest was observed in one patient (III-1, 2nd family). Overall, in the 12-lead ECG at rest, mean QTc was 423 ± 37 ms and median QTc was 422 (392; 454) ms. Abnormal Tpeak-Tend and Tpeak-Tend/QT ratio values or those related to high arrhythmic risk were not observed in the cohort. Upon standing briskly, four patients (44%) developed penetration in the 12-lead ECG. Mean QTc was 453 ± 18 ms and median QTc was 459 (439; 466) ms when standing briskly. During the 4th minute of the recovery phase of the EST, four patients (44%) developed diagnostic QTc prolongation of > 480 ms. The mean observed QTc during the 4th minute of the recovery phase of the EST was 485 ± 22 ms and the median was 478 (472; 503) ms. During the peak exercise phase, eight patients (89%) developed QTc prolongation of > 480 ms. Mean QTc was 497 ± 26 ms and median

Table 1 Comparison of clinical and electromechanical phenotype of the variant carriers

No	III-1, 1st	III-3, 1st	II-1, 2nd	III-1, 2nd	III-5, 2nd	III-6, 2nd	I-2, 3rd	I-1, 4th	II-1, 5th
Sex	M	M	F	F	M	F	F	M	M
Onset of symptoms, years	14	none	none	none	11	10	none	none	16
Age at molecular diagnosis, years	35	32	45	13	25	19	33	45	18
Age during clinical evaluation, years	38	34	49	18	29	23	39	47	24
Syncope/presyncope with stress	presyncope	none	none	none	syncope	presyncope	none	none	presyncope
Resting QTc[a], ms	374	437	452	468	447	427	417	416	409
Brisk standing QTc[a], ms	437	452	462	437	469	459	421	473	465
EST peak exercise QTc[a], ms	504	532	482	481	483	520	447	513	511
EST 4th min of recovery QTc[a], ms	463	490	478	510	474	503	454	517	472
Tpeak-Tend, ms	40	80	67	80	80	80	80	80	40
Tpeak-Tend/QT ratio	0.11	0.22	0.16	0.18	0.18	0.27	0.22	0.18	0.11
GLS, %	−20.1	−17.4	−21.6	−22.7	−20.4	−21.5	−24.7	N/A	N/A
EMW, ms	0	−37	−13	−8	−14	−18	19	N/A	N/A
Longitudinal mechanical dispersion, ms	27	41	26	32	37	20	34	N/A	N/A

EMW Electromechanical window, *EST* Exercise stress test, *F* Female, *GLS* Global longitudinal strain, *M* Male, *SCD* Sudden cardiac death

[a]corrected QT values were calculated using the Bazett formula

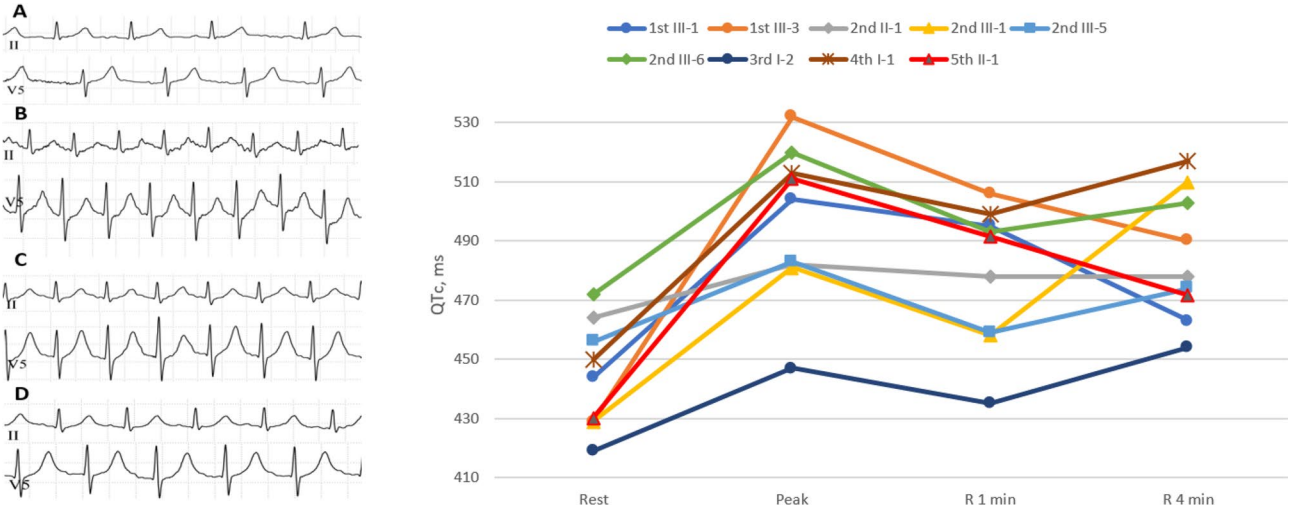

Fig. 2 Left: III-3 1 st family member QTc dynamics* in 12-lead ECG during EST. **A** PRETEST/at rest HR = 86 bpm, QTc 429 ms; (**B**) 200 W/peak exercise HR = 163 bpm, QTc 532 ms; (**C**) 1 st min of recovery HR = 150 bpm, QTc 506 ms; (**D**) 4th min of recovery HR = 115 bpm, QTc 490 ms. Right: grafical QTc dynamics of all patients during exercise stress test. HR – heart rate, bpm – beats per minute, R 1 min – 1 st min of recovery; R 4 min – 4th min of recovery. * RR-QT couples measured in lead II, corrected with the Bazett formula and average provided

QTc was 504 (482; 513) ms during this stage of the EST (Fig. 2).

All patients had normal LV ejection fraction (> 55%) and no concomitant structural heart disease or signs of myocardial ischemia during transthoracic echocardiography. LV strain analysis was performed, and the electromechanical window (EMW) was calculated in seven patients from the cohort. The data of two patients was lost during the image transmission process. One patient had reduced global longitudinal strain (GLS) (III-3, 2nd family, GLS − 17.4%). The rest had GLS within normal ranges. Significant longitudinal mechanical dispersion was observed in three patients (43%). The mean value of longitudinal mechanical dispersion was 31.0 ± 7.2 ms. A majority of the patients (71%) had negative EMW.

One patient (I-2, 3rd family) in the cohort was asymptomatic, and her electromechanical parameters remained in the normal range during the entire clinical evaluation.

Genetic findings

Heterozygous *KCNQ1* variant NM_000218.3:c.1111G > C, NP_000209.2:p.(Ala371Pro), (rs199473412) was detected in 2 probands from 3rd and 5th families by next-generation sequencing and seven other individuals from 1 st – 4th families by Sanger sequencing. There are reports of alternative pathogenic variant c.1111G > A disrupting the same amino acid residue in *KCNQ1* and possibly resulting in p.(Ala371Thr) substitution [26–29]. *KCNQ1* variant c.1111G > C was not found in the gnomAD v4.0.0 database [30]. ClinVar includes an entry for

this genomic variant (ID: 237221). In silico analysis predicted that this variant in a protein's sequence is likely to cause functional damage: PolyPhen—possibly pathogenic (1), Sift—pathogenic (0), MutT—pathogenic (0.99), AlphaMissense predicts the variant as pathogenic (0.999) [31]. The variant is classified as pathogenic according to ACMG criteria (14 points: PM1 strong, PM5 strong, PP3 strong, PM2 supporting, PP5 supporting).

Protein structure analysis and molecular dynamics simulations

KCNQ1 is a transmembrane protein, forming a tetrameric potassium channel. Each KCNQ1 subunit binds calmodulin, an obligatory subunit of the channel, and other regulatory subunits (KCNEs 1–5) and signaling lipid phosphatidylinositol 4,5-bisphosphate [15, 30]. In the known experimental structures of KCNQ1, the protein forms a domain-swapped tetramer in the membrane, and each KCNQ1 subunit interacts with one calmodulin molecule in the cytosolic part (Fig. 3, A). Residue 371 is located at this KCNQ1-calmodulin interaction interface.

To investigate possible impacts of the p.Ala371Pro substitution on the protein structure, 500 ns molecular dynamics simulations were performed on wild-type and mutant protein fragments. Each simulation was done in three copies to ensure the reproducibility of the calculations. Root Mean Square Deviations (RMSD) from the initial structure show that simulations converge to equilibrium, with the RMSDs in the last 100 ns of the simulation being between 2.5 and 3 Å (not shown). The 500 ns snapshots from the six runs are displayed in Fig. 3B. Partial unwinding of the helical structure is visible where the altered residue 371 is located after introducing the change from alanine to proline. HA helix has been shown to participate in significant and conserved conformational changes, necessary for proper KCNQ1 functioning [15]. According to these simulation results, the substitution p.Ala371Pro may disrupt the structure and impact the protein function.

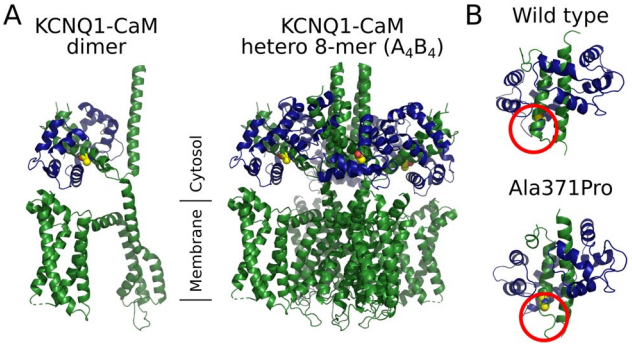

Fig. 3 The structure of KCNQ1-calmodulin (CaM) complex (PDB:6UZZ) (**A**) and the results of molecular dynamics simulations of the protein fragment involving the p.Ala371Pro substitution (**B**). KCNQ1 is green, calmodulin is blue, and the altered residue 371 is shown in yellow spheres. Predicted structural differences between two protein forms are highlighted in red circles

Another pathogenic variant of the same residue has been reported, p.Ala371Thr [26–29]. To compare the structural consequences of these two substitutions, we also performed simulations of the p.Ala371Thr variant using the same protocol. We compared the α-helix occupancies for residues 366–376, the helix starting position, and contacts of the residue 371 with calmodulin (Suppl. Mat. 4 Table S1). According to the simulation results, the variant p.Ala371Thr does not affect the α-helix, but both variants seem to form more contacts with calmodulin than the wild-type protein. Moreover, additional hydrogen bonding was observed in our models of the p.Ala371Thr variant, which can also affect the protein function (Suppl. Mat. 4 Fig. S1). Thus, at the structural level the newly reported substitution p.Ala371Pro seems different from the previously known variant p.Ala371Thr.

Functional evaluation

Identification and selection of cells expressing KCNQ1

Pathogenic variants in KCNQ1 alter the I_{Ks}, causing a prolonged QT interval [3] and, in rare cases, short QT syndrome [33, 34]. To investigate the functional effects of the p.(Ala371Pro) variant in KCNQ1, HEK293 cells were transfected with either wild-type (WT) or mutant (A371P) KCNQ1 channels together with KCNE1 subunit. Transfected cells expressing KCNQ1 or KCNE1 were identified for electrophysiological analysis based on CyOFP1 fluorescence (co-expressed with KCNQ1) or EGFP fluorescence (co-expressed with KCNE1) (Fig. 4).

KCNQ1 variant causes a significant reduction in current density

In the heart, the functional Kv7.1 channels are assembled with KCNE1 subunits, which substantially alter the function and biophysical properties of the channel. KCNE1 notably enhances KCNQ1 current amplitude [3, 35, 36]. Given this, we examined how A371P influence the electrophysiological properties of KCNQ1 + KCNE1 channels.

Representative current traces of HEK293 cells transfected with WT + KCNE1 and A371P + KCNE1 are presented in Fig. 5, A. Significant differences between current densities of tested groups were observed even at + 10 mV and became progressively larger with increasing depolarization steps (Fig. 5, B). At + 30 mV, WT + KCNE1 produced a significantly higher current density (15.8 ± 1.09, pA/pF, $n = 11$) than A371P + KCNE1 (10.84 ± 0.48 pA/pF, $n = 24$, Fig. 5, B). At + 70 mV, this difference was even higher, 33.92 ± 2.44 pA/pF, $n = 11$ in WT + KCNE1 and 19.87 ± 0.86 pA/pF, $n = 24$ in A371P + KCNE1 (Fig. 5, B). These findings demonstrate

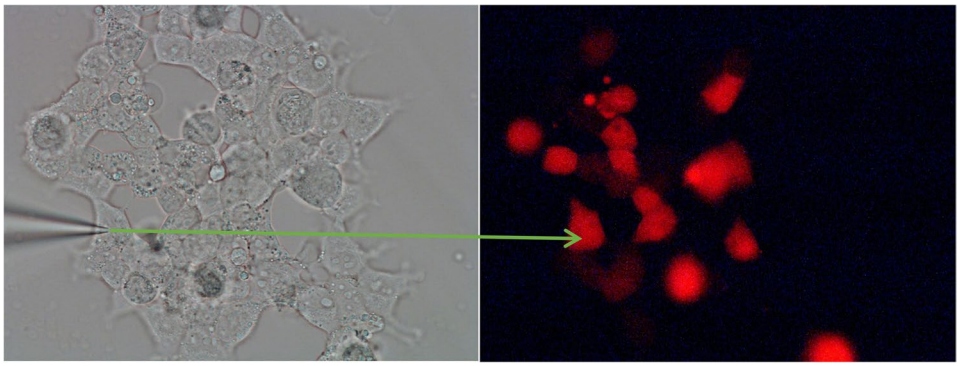

Fig. 4 Left: Light microscopy image showing cell patched with a microelectrode. Right: Fluorescence microscopy image of the same field of view, with an arrow indicating the CyOFP1-positive patched cell

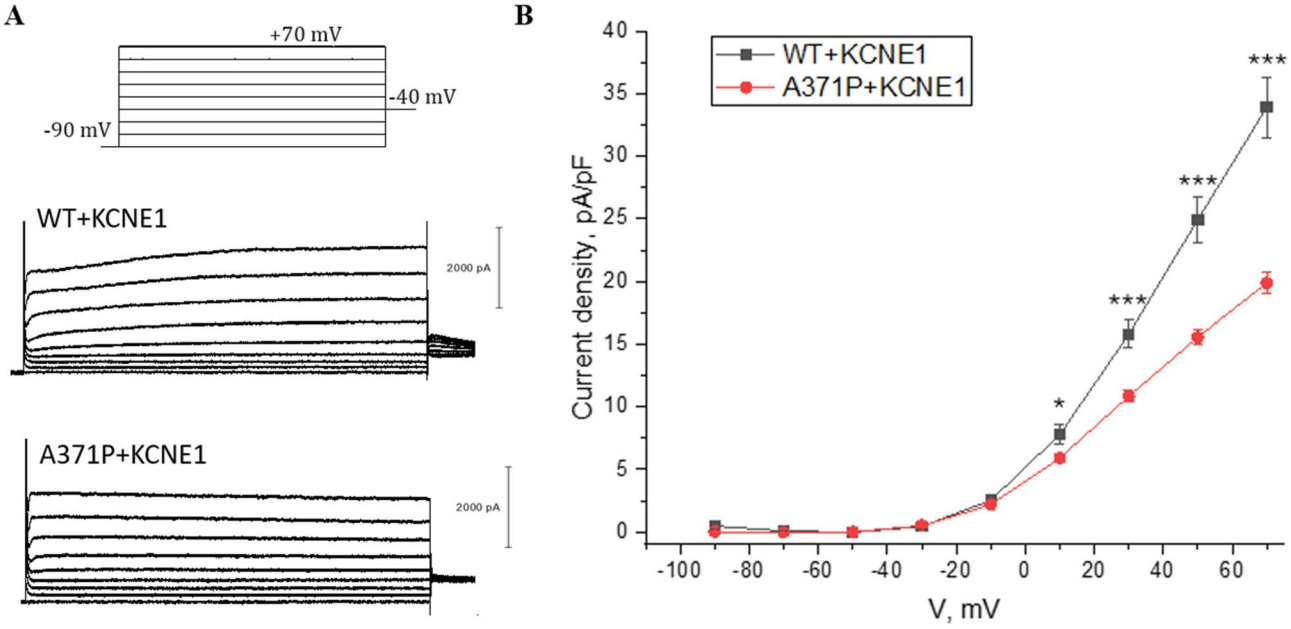

Fig. 5 **A** Patch clamp analysis of I_{Ks} in HEK293 cells transfected with WT + KCNE1 or A371P + KCNE1. **A** *Upper panel*: The voltage-clamp protocol that starts from a holding potential of −90 mV and depolarizing steps of 2-s duration and applied in 20 mV increments up to + 70 mV. *Lower panels*: Representative whole-cell current traces. **B** Dependence of current density on membrane potential (I–V) for the indicated groups. The number of cells in each condition is specified in the text. Data are shown as mean ± SEM. *$p \leq 0.05$, ***$p \leq 0.005$

that the A371P led to a partial loss-of-function in channels formed by co-expression of KCNQ1 + KCNE1.

Chromanol sensitivity of altered KCNQ1/KCNE1 channels

To verify the origin of observed outward currents, we tested the sensitivity of these currents to chromanol 293B, a selective KCNQ1 blocker. The current density observed in cells co-expressing WT + KCNE1 was significantly reduced by chromanol to 10.7 ± 3.98 pA/pF, (n = 6; Fig. 6) at + 70 mV, confirming the contribution of currents mediated by KCNQ1 channels. Moreover, A371P + KCNE1 was also sensitive to chromanol: current density was significantly reduced to 10.86 ± 1.45 pA/pF, at + 70 mV (n = 7; Fig. 6). These results suggest that, although A371P reduces current density, the channel remains chromanol sensitive.

The effects of KCNQ1 variant on the activation and conductance of the channel

Reduced current density in A371P + KCNE1 may be due to reduced channel conductance or shifted voltage dependency. A371P + KCNE1 did not alter the voltage dependence of activation compared to WT + KCNE1 ($V_1/_2$: −21.16 ± 1.57 mV, n = 24 for A371P + KCNE1 vs. −15.49 ± 2.1 mV, n = 11 for WT + KCNE1; Fig. 7A, C). However, the maximal conductance ($G_{max)}$ was significantly reduced in A371P + KCNE1 (0.27 ± 0.01 nS/pF, n = 24) compared to WT + KCNE1 (0.5 ± 0.04 nS/pF, n = 11) (Fig. 7A, B). These findings demonstrate that

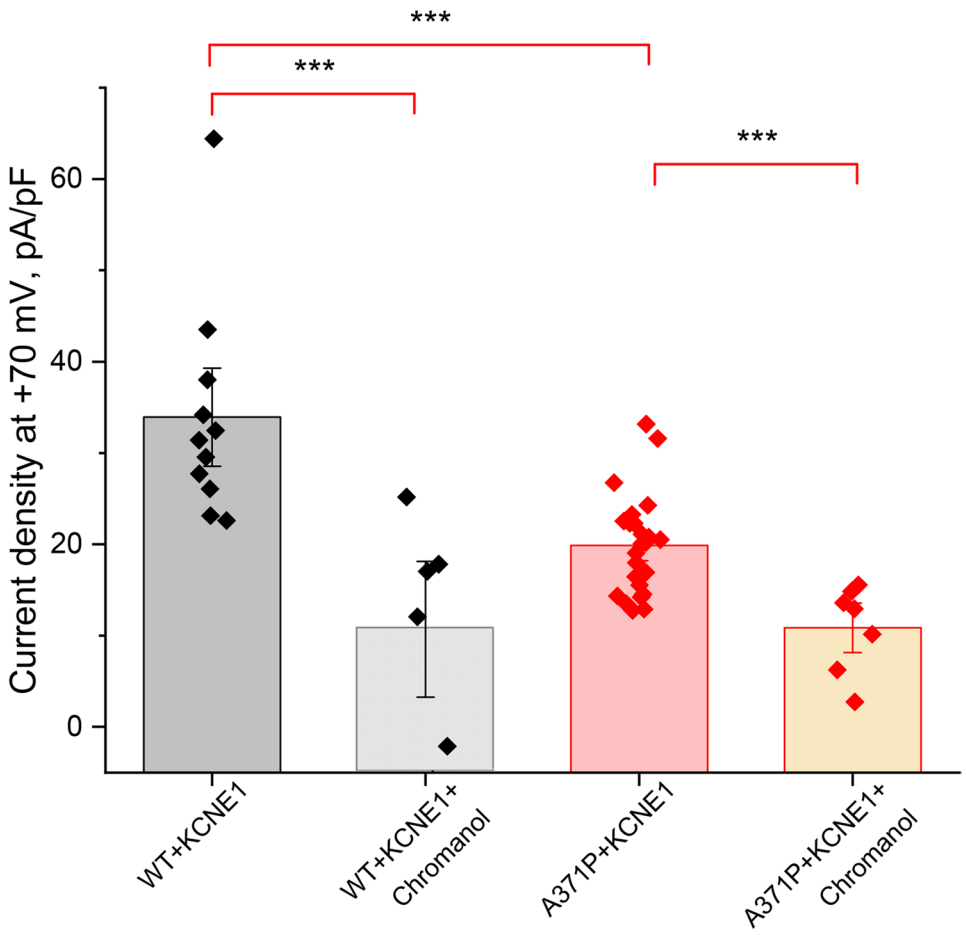

Fig. 6 Current densities (pA/pF) at + 70 mV in HEK293 cells transfected with WT + KCNE1 or A371P + KCNE1 with and without Chromanol 293B (10 μM). Chromanol 293B was applied to block the KCNQ1 current. Bars represent mean ± SEM; each diamond corresponds to an individual cell. ***$p \leq 0.005$

A371P disrupts normal channel gating by decreasing the maximal conductance.

Discussion

The *KCNQ1* variant c.1111G > C that results in the substitution p.(Ala371Pro) was identified in our recent analysis of clinical, electrical, and mechanical characteristics of congenital LQTS (*KCNQ1* and *KCNH2* variants) in Lithuania [37]. The variant was identified in 5 seemingly unrelated Lithuanian families, presuming a possibility of a common ancestor with a founder mutation in our population, which is to be clarified in further experiments. In this article, we provide a detailed clinical analysis of adult individuals with the c.1111G > C variant in *KCNQ1* and the results of functional experiments confirming the negative impact of the amino acid alteration.

The clinical features of nine tested individuals from five families were heterogeneous, from one asymptomatic individual with all electromechanical parameters normal to four individuals with symptoms during physical activities in childhood or puberty. There were sudden cardiac deaths of two females at a young age. The QTc in a 12-lead ECG at rest was not informative, because only one patient had QTc prolongation there. QTc interval prolongation was a "hallmark" of the disease for decades, and yet, according to the modified LQTS diagnostic score [38], the clinical diagnosis can be made from repetitive prolonged QTc values. However, Wilde et al. provided insight that "a single QTc will never be able to distinguish all non-LQTS ECGs from all LQTS ECGs" [39]. Furthermore, it is also known from previous studies that the QTc interval may be within normal range in up to 40% of all genotype-positive individuals [40]. At peak exercise phase during the EST, all our patients except one developed pathological QTc prolongation (from 481 to 532 ms) that failed to shorten properly in the recovery phase. The cohort demonstrated a QTc adaptation pattern unique for the LQT1 during exercise and early recovery of the EST as a consequence of the dysfunctional I_{Ks} channels, causing paradoxical QTc prolongation related to adrenergic stimulation at fast heart rates.

However, risk assessment of the individual currently relies not only on electrical parameters like the QTc, but also clinical, genetic, and mutation-specific determinants

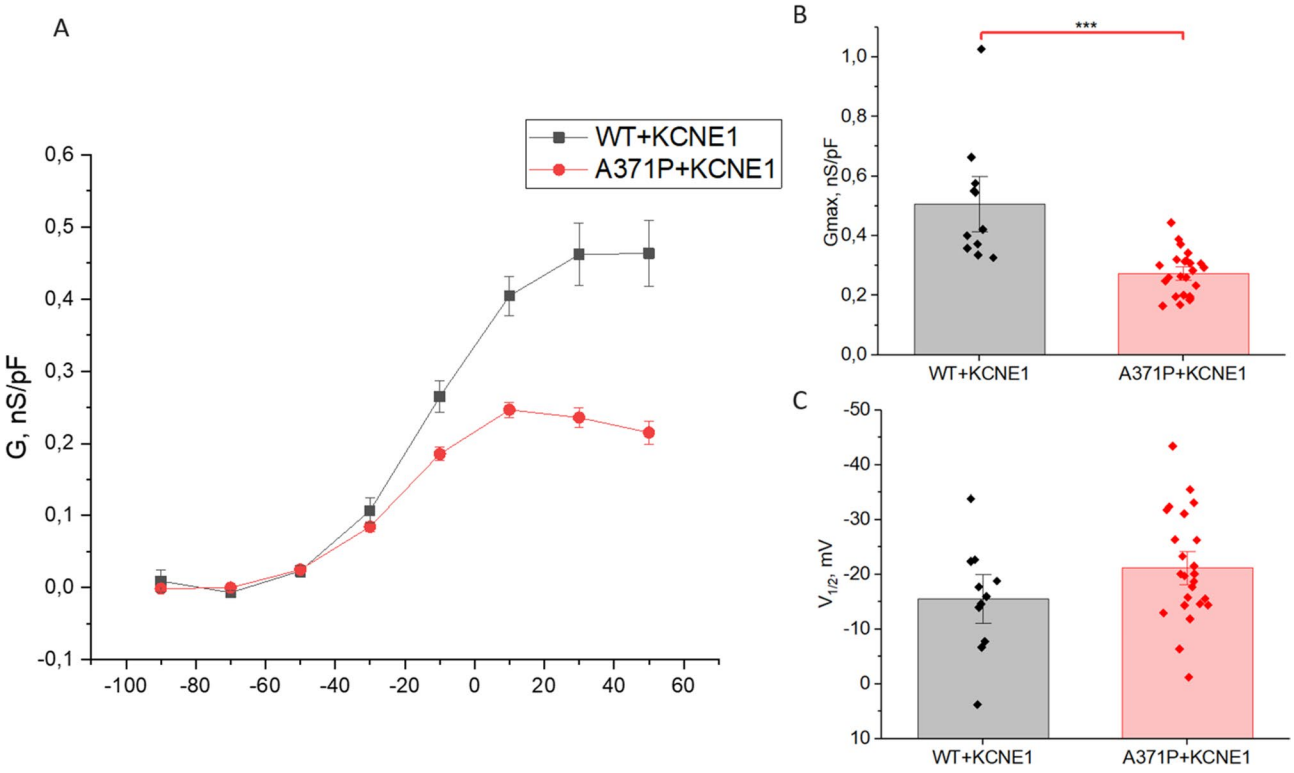

Fig. 7 Activation of currents mediated in HEK293 cells transfected with WT + KCNE1 and A371P + KCNE1. **A** Voltage dependence of conductance. Symbols with error bars represent mean ± SEM. **B** The maximal conductance (G_{max}). **C** The mid-point of the activation curve ($V_{1/2}$). Bars represent mean ± SEM; each diamond corresponds to an individual cell. ***$p \leq 0.005$

[41]. Electromechanical parameters in LQTS were introduced recently [42–44]. Accumulating evidence [41, 43, 45] demonstrates that LQTS is linked to subclinical global and regional ventricular mechanical abnormalities. Sugrue et al. validated the EMW, a mismatch between the end of electrical and mechanical systole, as a risk factor in LQTS and showed that it outperformed the heart rate-corrected QT interval as a predictor of symptomatic status [45]. In our study, the majority of patients had slightly negative EMW. Longitudinal mechanical dispersion, which is thought to mirror the electrical heterogeneity arising from prolonged subendocardial Purkinje fibers action potentials, is also known to be longer in LQTS patients compared with healthy individuals [43]. Several (43%) of our patients had a longitudinal mechanical dispersion value ≥ 33 ms, which by Haugaa et al. was proposed to identify LQTS mutation carriers with a history of events [43].

Observed results of the clinical evaluation of the *KCNQ1* p.(Ala371Pro) variant carriers can be supportive of a pathogenic role of the variant, but any parameter cannot be conclusive in isolation. A comprehensive approach employing electromechanical parameters, clinical signs, and genetic information for understanding variant pathogenicity, in line with functional and structural data, should be used.

The *KCNQ1* p.(Ala371Thr) pathogenic variant has been previously reported in one family [26]. According to limited clinical data, the mean QTc in two individuals with p.(Ala371Thr) was 506 ms, and sudden death before 40 years occurred in one of three individuals. Variants in nearby residues p.(Ser373Pro) and p.(Leu374His) have been reported as pathogenic [46]. The variant p.(Ser373Pro) was detected in seven members of a Dutch family [46]. The QTc values of the carriers varied from 422 to 540 ms (at rest), and sudden deaths of children were reported, meanwhile most of the family members with the p.(Leu374His) variant had severe QT interval prolongation with symptoms observed since the age of one [47].

The *KCNQ1* variant p.(Ala371Pro) is located in the proximal part of helix A of the C-terminal region of Kv7.1. Helices HA and HB interact with calmodulin, an essential player in channel function and disease biology [48]. Association with calmodulin is necessary for proper channel assembly and function [49]. Kapplinger et al. provided a conservation analysis and an extensive case-control topology-based study identifying three regions of high conservation (CR) within the C-terminal regions of Kv7.1 that have a high probability of LQT1 pathogenicity: CR1 (residues 349–391), CR2 (residues 509–575), and CR3 (residues 585–607) [50]. Although missense

pathogenic variants are most commonly detected in the CR2 region, variants in CR1 may also profoundly affect on protein structure and function. While our analysis of protein structure and molecular dynamics simulations does not provide evidence that the p.Ala371Pro substitution directly alters CaM binding, it suggests possible protein conformational changes. Furthermore, functional studies showed that an alternative p.Ala371Thr substitution impaired CaM binding and disrupted channel expression [27]. Another study demonstrated that p.Ala371Thr substitution may affect channel function via perturbed interactions with the C-terminus of KCNE1 [29]. Yet, our molecular dynamics simulations results suggest that the structural consequences of the newly reported Pro and previously known Thr substitutions of the residue Ala371 might be partially different. Using bacterial expression constructs, Gosh et al. also did not detect any interaction between calmodulin and KCNQ1 with the p.(Ser373Pro) mutation [51]. Moreover, when expressed in oocytes, KCNQ1 channels with p.(Ser373Pro) failed to generate K^+ currents differently from those recorded from uninjected control oocytes over a range of test potentials from − 60 to + 60 mV, suggesting that changes in calmodulin interaction with the KCNQ1 C-terminus may predispose to LQT1 [51]. Functional characterization of the p.(Leu374His) substitution revealed that I_{Ks}-Leu374His exhibited a complete loss of function compared to the WT channel [47]. Thus, the results of both our computational modeling and previous experimental studies of the nearby residues and an alternative change in this position suggest that the substitution p.(Ala371Pro) may affect the function of the protein.

QTc prolongation is associated with the reduction of I_{Ks} current density, which is generated by the KCNQ1 channel when co-expressed with the accessory β-subunit KCNE1. To evaluate I_{Ks} channel functionality, the complex of KCNQ1 + KCNE1 is usually used [35, 36, 52]. Our results showed that the p.(Ala371Pro) KCNQ1 variant co-expressed with KCNE1 reduced current density at + 70 mV by about 40%, indicating partial loss of function. Moreover, the remaining current density was still chromanol sensitive. The reduction in current density observed with the p.(Ala371Pro) KCNQ1 variant co-expressed with KCNE1 is consistent with previous studies showing that various KCNQ1 pathogenic variants lead to decreased I_{Ks}. For example, pathogenic variants in the C-terminal region of KCNQ1 co-expressed with KCNE1, such as p.(Arg555Cys), besides a reduction in current density, also cause a marked rightward shift in the voltage dependence of activation [53]. Similarly, several other C-terminal mutants co-expressed with KCNE1, including p.(Arg555His), p.(Ala590Thr), and p.(Gly589Asp), have been shown to reduce I_{Ks} current density and shift the voltage dependence of activation to more positive potentials [54–56]. In contrast, some pathogenic variants, such as p.(Pro535Thr), do not alter voltage dependence but reduce maximal conductance [57]. In this study, the detected variant did not affect the voltage dependence of activation but reduced the maximal conductance of the channel by 46%. The reported variant results in a partial loss of function of KCNQ1 channels, which is compatible with observed LQT1 phenotypic features.

In our experiments, we investigated the homozygous form of the p.(Ala371Pro) variant, yet in clinical settings both homozygous and heterozygous carriers are observed. This distinction is clinically relevant, as differences in zygosity can influence the severity of the phenotype and may involve mechanisms such as dominant negative effects. In this study, we focused on the direct impact of the p.(Ala371Pro) variant on potassium currents. Whether the p.(Ala371Pro) variant exerts a dominant negative effect is currently unknown. Heterozygous patients often exhibit a very mild phenotype, while homozygous individuals show more severe symptoms [58]. However, dominant negative effects cannot be excluded, as illustrated by the ΔF275 alteration, which strongly suppresses I_{Ks} function and leads to an LQT1 phenotype [59]. Therefore, our study addressed the variant's direct functional consequences, while the potential effects of heterozygosity and dominant negative interactions remain important topics for future investigation.

Conclusions

This is the first functional description of the *KCNQ1* variant c.1111G > C causing LQT1 phenotypic features. This pathogenic variant of the KCNQ1 channel disrupts its normal functionality by decreasing the conductance, which results in partial loss of function. The variant highly suggests the risk of disease-related cardiac events, particularly under adrenergic urge, predisposed by the topology of genetic alteration in the Kv7.1 protein structure in the C-terminus helix HA.

Abbreviations

A371P	p.(Ala371Pro) variant
CR	Regions of high conservation
DNA	Deoxyribonucleic acid
ECG	Electrocardiogram
EMW	Electromechanical window
EST	Exercise stress test
GLS	Global longitudinal strain
GFP	Green fluorescent protein
HEK	Human embryonic kidney
LQTS	Long QT syndrome
LQT1	Long QT syndrome Type 1
LV	Left ventricle
PCR	Polymerase chain reaction
WT	Wild-type

Supplementary Information

The online version contains supplementary material available at https://doi.org/10.1186/s12872-025-05335-x.

Supplementary Material 1: Description of genealogies of 1st-5th families

Supplementary material 2: Methods of clinical evaluation

Supplementary material 3: The genes, analysed using TruSight Cardio Sequencing panel

Supplementary material 4: MD trajectory analysis

Acknowledgements
The authors thank to the patients for their contribution.

Authors' contributions
EP, MV, AA, AS, VK, JD and JB were responsible for the methodology of the study. NB, EP and JB were responsible for the clinical data collection and analysis. AJ performed plasmid mutagenesis, bacterial cloning. GP, VZ performed cell transfection. VK, JD performed analysis of protein sequence and structure. AA designed and supervised an electrophysiological experiment. ASh performed the electrophysiological experiment. EP, NB, ASh, AA, AS, ZM and JD drafted the article. NB, EP, AA, ASh, AS, JD, VK, VM, GP and JB participated in manuscript writing and reviewed the paper. All authors approved the final version of the manuscript.

Funding
This research was funded by a grant (No. S-MIP-21–15; ATGC project) from the Research Council of Lithuania (EP).

Data availability
All the data in this report are available from the corresponding author upon a reasonable request. Molecular Dynamics simulations workflow and data were deposited to Zenodo doi: https://doi.org/10.5281/zenodo.17348568.

Declarations

Ethics approval and consent to participate
The study was approved by the Vilnius Regional Biomedical Research Ethics Committee of Lithuania (Protocol Code No. 2020/1-1182-669, date of approval January 28, 2020; and No. 2021/9-1373-849, date of approval September 21, 2021). All procedures involving human participants followed the Helsinki Declaration. All subjects gave their informed consent for participation in this study.

Consent for publication
Not applicable.

Competing interests
The authors declare no competing interests.

Received: 23 May 2025 / Accepted: 31 October 2025
Published online: 26 November 2025

References

1. Liang JJ, Callans DJ. Electrophysiologic testing and cardiac mapping. In: Kowey P, Piccini JP, Naccarelli G, Reiffel JA, editors. Cardiac Arrhythmias, pacing and sudden death [Internet]. Cham: Springer International Publishing; 2017. pp. 75–86. [cited 2024 Aug 22]. https://doi.org/10.1007/978-3-319-58000-5_7.
2. Morgat C, Fressart V, Porretta AP, Neyroud N, Messali A, Temmar Y, et al. Genetic characterization of KCNQ1 variants improves risk stratification in type 1 long QT syndrome patients. Europace. 2024;26:euae136. https://doi.org/10.1093/europace/euae136.
3. Barhanin J, Lesage F, Guillemare E, Fink M, Lazdunski M, Romey G. KvLQT1 and IsK (minK) proteins associate to form the IKS cardiac potassium current. Nature. 1996;384:78–80. https://doi.org/10.1038/384078a0.
4. Wu J, Ding W-G, Horie M. Molecular pathogenesis of long QT syndrome type 1. J Arrhythm. 2016;32:381–8. https://doi.org/10.1016/j.joa.2015.12.006.
5. Ponce-Balbuena D, Deschênes I. Long QT syndrome - bench to bedside. Heart Rhythm O2. 2021;2:89–106. https://doi.org/10.1016/j.hroo.2021.01.006.
6. Schwartz PJ, Moreno C, Kotta M-C, Pedrazzini M, Crotti L, Dagradi F, et al. Mutation location and IKs regulation in the arrhythmic risk of long QT syndrome type 1: the importance of the KCNQ1 S6 region. Eur Heart J. 2021;42:4743–55. https://doi.org/10.1093/eurheartj/ehab582.
7. Vanoye CG, Thompson CH, Desai RR, DeKeyser J-M, Chen L, Rasmussen-Torvik LJ, et al. Functional evaluation of human ion channel variants using automated electrophysiology. Methods Enzymol. 2021;654:383–405. https://doi.org/10.1016/bs.mie.2021.02.011.
8. Steinhaus R, Proft S, Schuelke M, Cooper DN, Schwarz JM, Seelow D. MutationTaster2021. Nucleic Acids Res. 2021;49:W446–51. https://doi.org/10.1093/nar/gkab266
9. Adzhubei IA, Schmidt S, Peshkin L, Ramensky VE, Gerasimova A, Bork P, et al. A method and server for predicting damaging missense mutations. Nat Methods. 2010;7:248–9. https://doi.org/10.1038/nmeth0410-248.
10. Sim N-L, Kumar P, Hu J, Henikoff S, Schneider G, Ng PC. SIFT web server: predicting effects of amino acid substitutions on proteins. Nucleic Acids Res. 2012;40:W452–7. https://doi.org/10.1093/nar/gks539.
11. Ye J, Coulouris G, Zaretskaya I, Cutcutache I, Rozen S, Madden TL. Primer-BLAST: a tool to design target-specific primers for polymerase chain reaction. BMC Bioinformatics. 2012;13:134. https://doi.org/10.1186/1471-2105-13-134.
12. The UniProt Consortium. UniProt: the universal protein knowledgebase in 2025. Nucleic Acids Res. 2025;53:D609–17. https://doi.org/10.1093/nar/gkae1010.
13. Dapkūnas J, Timinskas A, Olechnovič K, Tomkuvienė M, Venclovas Č. PPI3D: a web server for searching, analyzing and modeling protein–protein, protein–peptide and protein–nucleic acid interactions. Nucleic Acids Res. 2024;52:W264–71. https://doi.org/10.1093/nar/gkae278.
14. Dapkūnas J, Venclovas Č. Template-Based modeling of protein complexes using the PPI3D web server. In: Kihara D, editor. Protein structure prediction [Internet]. New York, NY: Springer US; 2020. pp. 139–55. [cited 2025 May 20]. https://doi.org/10.1007/978-1-0716-0708-4_8.
15. Sun J, MacKinnon R. Structural basis of human KCNQ1 modulation and gating. Cell Elsevier. 2020;180:340–7. https://doi.org/10.1016/j.cell.2019.12.003.e9.
16. Abraham MJ, Murtola T, Schulz R, Páll S, Smith JC, Hess B, et al. GROMACS: high performance molecular simulations through multi-level parallelism from laptops to supercomputers. SoftwareX. 2015;1:19–25. https://doi.org/10.1016/j.softx.2015.06.001.
17. Huang J, Rauscher S, Nawrocki G, Ran T, Feig M, de Groot BL, et al. CHARMM36m: an improved force field for folded and intrinsically disordered proteins. Nat Methods. 2017;14:71–3. https://doi.org/10.1038/nmeth.4067.
18. Jorgensen WL, Chandrasekhar J, Madura JD, Impey RW, Klein ML. Comparison of simple potential functions for simulating liquid water. J Chem Phys. 1983;79(2):926–35. https://doi.org/10.1063/1.445869.
19. Grant BJ, Rodrigues APC, ElSawy KM, McCammon JA, Caves LSD. Bio3d: an R package for the comparative analysis of protein structures. Bioinformatics. 2006;22:2695–6. https://doi.org/10.1093/bioinformatics/btl461.
20. Kabsch W, Sander C. Dictionary of protein secondary structure: pattern recognition of hydrogen-bonded and geometrical features. Biopolymers. 1983;22:2577–637. https://doi.org/10.1002/bip.360221211.
21. Olechnovič K, Venclovas C, Voronota. A fast and reliable tool for computing the vertices of the Voronoi diagram of atomic balls. J Comput Chem. 2014;35:672–81. https://doi.org/10.1002/jcc.23538.
22. Ooi A, Wong A, Esau L, Lemtiri-Chlieh F, Gehring C. A guide to transient expression of membrane proteins in HEK-293 cells for functional characterization. Front Physiol. 2016;7:300. https://doi.org/10.3389/fphys.2016.00300.
23. Inada M, Izawa G, Kobayashi W, Ozawa M. 293 cells express both epithelial as well as mesenchymal cell adhesion molecules. Int J Mol Med. 2016;37:1521–7. https://doi.org/10.3892/ijmm.2016.2568.
24. Thomas P, Smart TG. HEK293 cell line: a vehicle for the expression of recombinant proteins. J Pharmacol Toxicol Methods. 2005;51:187–200. https://doi.org/10.1016/j.vascn.2004.08.014.
25. Aidery P, Kisselbach J, Schweizer PA, Becker R, Katus HA, Thomas D. Impaired ion channel function related to a common *KCNQ1* mutation — Implications for risk stratification in long QT syndrome 1. Gene. 2012;511:26–33. https://doi.org/10.1016/j.gene.2012.09.041.

26. Donger C, Denjoy I, Berthet M, Neyroud N, Cruaud C, Bennaceur M. KVLQT1 C-terminal missense mutation causes a forme fruste long-QT syndrome. Circulation. 1997;96:2778–81. https://doi.org/10.1161/01.cir.96.9.2778.
27. Shamgar L, Ma L, Schmitt N, Haitin Y, Peretz A, Wiener R, et al. Calmodulin is essential for cardiac IKS channel gating and assembly: impaired function in long-QT mutations. Circ Res. 2006;98:1055–63. https://doi.org/10.1161/01.RES.0000218979.40770.69.
28. Splawski I, Shen J, Timothy KW, Lehmann MH, Priori S, Robinson JL, et al. Spectrum of mutations in long-QT syndrome genes. KVLQT1, HERG, SCN5A, KCNE1, and KCNE2. Circulation. 2000;102:1178–85. https://doi.org/10.1161/01.cir.102.10.1178.
29. Zheng R, Thompson K, Obeng-Gyimah E, Alessi D, Chen J, Cheng H, et al. Analysis of the interactions between the C-terminal cytoplasmic domains of KCNQ1 and KCNE1 channel subunits. Biochem J. 2010;428:75–84. https://doi.org/10.1042/BJ20090977.
30. Karczewski KJ, Francioli LC, Tiao G, Cummings BB, Alföldi J, Wang Q, et al. The mutational constraint spectrum quantified from variation in 141,456 humans. Nature. 2020;581:434–43. https://doi.org/10.1038/s41586-020-2308-7.
31. Cheng J, Novati G, Pan J, Bycroft C, Žemgulytė A, Applebaum T, et al. Accurate proteome-wide missense variant effect prediction with alphamissense. Science. 2023;381:eadg7492. https://doi.org/10.1126/science.adg7492.
32. Sun J, MacKinnon R. Cryo-EM structure of a KCNQ1/CaM complex reveals insights into congenital long QT syndrome. Cell. 2017;169:1042–e10509. https://doi.org/10.1016/j.cell.2017.05.019.
33. Bellocq C, van Ginneken ACG, Bezzina CR, Alders M, Escande D, Mannens MMAM, et al. Mutation in the KCNQ1 gene leading to the short QT-interval syndrome. Circulation. 2004;109:2394–7. https://doi.org/10.1161/01.CIR.0000130409.72142.FE.
34. Hedley PL, Jørgensen P, Schlamowitz S, Wangari R, Moolman-Smook J, Brink PA, et al. The genetic basis of long QT and short QT syndromes: a mutation update. Hum Mutat. 2009;30:1486–511. https://doi.org/10.1002/humu.21106.
35. Nakajo K, Kubo Y. KCNQ1 channel modulation by KCNE proteins via the voltage-sensing domain. J Physiol. 2015;593:2617–25. https://doi.org/10.1113/jphysiol.2014.287672.
36. Sanguinetti MC, Curran ME, Zou A, Shen J, Spector PS, Atkinson DL, et al. Coassembly of K(V)LQT1 and MinK (IsK) proteins to form cardiac I(Ks) potassium channel. Nature. 1996;384:80–3. https://doi.org/10.1038/384080a0.
37. Bileišienė N, Mikštienė V, Preikšaitienė E, Kažukauskienė I, Tarutytė G, Zakarkaitė D, et al. Clinical, electrical, and mechanical parameters in potassium channel-mediated congenital long QT syndrome. J Clin Med. 2025;14:2540. https://doi.org/10.3390/jcm14082540.
38. Zeppenfeld K, Tfelt-Hansen J, de Riva M, Winkel BG, Behr ER, Blom NA, et al. 2022 ESC guidelines for the management of patients with ventricular arrhythmias and the prevention of sudden cardiac death. Eur Heart J. 2022. https://doi.org/10.1093/eurheartj/ehac262.
39. Wilde AAM, Amin AS, Postema PG. Diagnosis, management and therapeutic strategies for congenital long QT syndrome. Heart. 2022;108:332–8. https://doi.org/10.1136/heartjnl-2020-318259.
40. Krahn AD, Laksman Z, Sy RW, Postema PG, Ackerman MJ, Wilde AAM, et al. Congenital long QT syndrome. JACC Clin Electrophysiol. 2022;8:687–706. https://doi.org/10.1016/j.jacep.2022.02.017.
41. Odening KE, van der Linde HJ, Ackerman MJ, Volders PGA, ter Bekke RMA. Electromechanical reciprocity and arrhythmogenesis in long-QT syndrome and beyond. Eur Heart J. 2022;43:3018–28. https://doi.org/10.1093/eurheartj/ehac135.
42. Deissler PM, Volders PGA, ter Bekke RMA. The electromechanical window for arrhythmia-risk assessment. Heart Rhythm. 2025;22:118–27. https://doi.org/10.1016/j.hrthm.2024.06.012.
43. Haugaa KH, Amlie JP, Berge KE, Leren TP, Smiseth OA, Edvardsen T. Transmural differences in myocardial contraction in long-QT syndrome: mechanical consequences of ion channel dysfunction. Circulation. 2010;122:1355–63. https://doi.org/10.1161/CIRCULATIONAHA.110.960377.
44. Borowiec K, Kowalski M, Kumor M, Duliban J, Śmigielski W, Hoffman P, et al. Prolonged left ventricular contraction duration in apical segments as a marker of arrhythmic risk in patients with long QT syndrome. Europace. 2020;22:1279–86. https://doi.org/10.1093/europace/euaa107.
45. Sugrue A, van Zyl M, Enger N, Mancl K, Eidem BW, Oh JK, et al. Echocardiography-guided risk stratification for long QT syndrome. J Am Coll Cardiol. 2020;76:2834–43. https://doi.org/10.1016/j.jacc.2020.10.024.
46. Jongbloed RJ, Wilde AA, Geelen JL, Doevendans P, Schaap C, Van Langen I, et al. Novel KCNQ1 and HERG missense mutations in Dutch long-QT families. Hum Mutat. 1999;13:301–10. https://doi.org/10.1002/(SICI)1098-1004(1999)13:4%3C301::AID-HUMU7%3E3.0.CO;2-V.
47. Hammami Bomholtz S, Refaat M, Buur Steffensen A, David J-P, Espinosa K, Nussbaum R, et al. Functional phenotype variations of two novel KV 7.1 mutations identified in patients with long QT syndrome. Pacing Clin Electrophysiol. 2020;43:210–6. https://doi.org/10.1111/pace.13870.
48. Dixit G, Dabney-Smith C, Lorigan GA. The membrane protein KCNQ1 potassium ion channel: functional diversity and current structural insights. Biochimica et Biophysica Acta (BBA). 2020;1862:183148. https://doi.org/10.1016/j.bbamem.2019.183148.
49. Novelli V, Faultless T, Cerrone M, Care M, Manzoni M, Bober SL, et al. Enhancing the interpretation of genetic observations in *KCNQ1* in unselected populations: relevance to secondary findings. Europace. 2023;25:euad317. https://doi.org/10.1093/europace/euad317.
50. Kapplinger JD, Tseng AS, Salisbury BA, Tester DJ, Callis TE, Alders M. Enhancing the predictive power of mutations in the C-terminus of the KCNQ1-encoded Kv7.1 voltage-gated potassium channel. J Cardiovasc Transl Res. 2015;8:187–97. https://doi.org/10.1007/s12265-015-9622-8.
51. Ghosh S, Nunziato DA, Pitt GS. KCNQ1 assembly and function is blocked by long-QT syndrome mutations that disrupt interaction with calmodulin. Circ Res. 2006;98:1048–54. https://doi.org/10.1161/01.RES.0000218863.44140.f2.
52. Barhanin J, Lesage F, Guillemare E, Fink M, Lazdunski M, Romey G. KvLQT1 and IsK (minK) proteins associate to form the IKS cardiac potassium current. Nature. 1996;384:78–80. https://doi.org/10.1038/384078a0.
53. Chouabe C, Neyroud N, Guicheney P, Lazdunski M, Romey G, Barhanin J. Properties of KvLQT1 K+channel mutations in Romano-Ward and Jervell and Lange-Nielsen inherited cardiac arrhythmias. EMBO J. 1997;16:5472–9. https://doi.org/10.1093/emboj/16.17.5472.
54. Aromolaran AS, Subramanyam P, Chang DD, Kobertz WR, Colecraft HM. LQT1 mutations in KCNQ1 C-terminus assembly domain suppress IKs using different mechanisms. Cardiovasc Res. 2014;104:501–11. https://doi.org/10.1093/cvr/cvu231.
55. Kinoshita K, Komatsu T, Nishide K, Hata Y, Hisajima N, Takahashi H, et al. A590T mutation in KCNQ1 C-terminal helix D decreases *I*ks channel trafficking and function but not Yotiao interaction. J Mol Cell Cardiol. 2014;72:273–80. https://doi.org/10.1016/j.yjmcc.2014.03.019.
56. Piippo K, Swan H, Pasternack M, Chapman H, Paavonen K, Viitasalo M, et al. A founder mutation of the potassium channel KCNQ1 in long QT syndrome: implications for Estimation of disease prevalence and molecular diagnostics. J Am Coll Cardiol. 2001;37:562–8. https://doi.org/10.1016/S0735-1097(00)01124-4.
57. González-Garrido A, Domínguez-Pérez M, Jacobo-Albavera L, López-Ramírez O, Guevara-Chávez JG, Zepeda-García O, et al. Compound heterozygous KCNQ1 mutations causing recessive Romano–Ward syndrome: functional characterization by mutant co-expression. Front Cardiovasc Med. 2021. https://doi.org/10.3389/fcvm.2021.625449.
58. Kinoshita K, Komatsu T, Nishide K, Hata Y, Hisajima N, Takahashi H, et al. A590T mutation in KCNQ1 C-terminal helix D decreases IKs channel trafficking and function but not Yotiao interaction. J Mol Cell Cardiol. 2014;72:273–80. https://doi.org/10.1016/j.yjmcc.2014.03.019.
59. Aizawa Y, Ueda K, Scornik F, Cordeiro JM, Wu Y, Desai M, et al. A novel mutation in KCNQ1 associated with a potent dominant negative effect as the basis for the LQT1 form of the long QT syndrome. J Cardiovasc Electrophysiol. 2007;18:972–7. https://doi.org/10.1111/j.1540-8167.2007.00889.x.

Publisher's note

Springer Nature remains neutral with regard to jurisdictional claims in published maps and institutional affiliations.